Characteristic Errors of the IMM Algorithm under Three Maneuver Models for an Accelerating Target

Chun Yang
Sigtem Technology, Inc.
San Mateo, CA 94402
chunyang@sigtem.com

Erik Blasch
Air Force Research Lab
WPAFB, OH 45433
erik.blasch@wpafb.afb.mil

Abstract – As a state-of-the-art algorithm, the Interacting Multiple Model (IMM) estimator is widely used for maneuvering target tracking. However, there still is uncertainty in how to design the multiple models used by an IMM estimator. In this context, this paper compares three maneuver models, namely, variable process noise, variable state dimension, and discrete acceleration inputs via computer simulations. The first two modeling techniques belong to the design approach using multiple bandwidths whereas the latter technique utilizes matched filters. The three models exhibit characteristic errors throughout a maneuver, which are termed n-, L-, and u-shaped, respectively. Compared to total root mean squared (RMS) errors, a time-equalized RMS (eRMS) may be more appropriate for a maneuvering target. The total and equalized RMS values are illustrated for the IMM under the three maneuver models for performance evaluation and filter tuning.

Keywords: IMM, Maneuver Models, Evaluation, Tuning.

1 Introduction

The multiple model approach is a viable technique widely used in signal processing, state estimation, and dynamic control. It is particularly suited for cases where signal and system models have large uncertainties and/or the models are subject to unknown changes over time. In the context of maneuvering target tracking, a target's maneuvers present such uncertainties because initiation and termination of a maneuver as well as the type and magnitude of maneuver are all unknown to a tracker.

A Kalman filter has an inherent ability to follow the changes in state (i.e., a tracking capability) partly from the state transition model (time update) and partly from the measurement update. In other words, a tracking filter fits a target motion model (e.g., of nearly constant velocity with acceleration noise) into noisy measurements. For a fixed model design, a filter has to compromise between dynamic responsiveness and steady state noise performance when changes occur inside the system. In contrast, multiple model approaches, exemplified by the Multiple Model Adaptive Estimator (MMAE) [11] and Interacting Multiple Model (IMM) algorithm [4], are data-driven variable-gain (adaptive) filters. Indeed, it is shown in [7] that the IMM outperforms the Kalman filter for large maneuver indexes.

A comprehensive survey of maneuvering target tracking using the multiple-model methods is available in [8]. A comparative study of various multiple model algorithms for tracking maneuvering targets is reported in [13] wherein seven algorithms, namely, the basic multiple model (MM) algorithm, a first order generalized pseudo Bayesian algorithm (GPB1), GPB2, IMM, B-best based MM algorithm, Viterbi-based MM algorithm, and re-weighted IMM, were compared but no clear winner was found among them. The multiple model algorithms and particularly the IMM algorithm and its variants have been extensively studied [9]. The IMM estimator is compared with the optimal estimator in [2]. Its performance is comparable to a GPB2 that uses N^2 Kalman filters per step but only requires the computation load of a GPB1 algorithm that only needs N Kalman filters per step where N is the number of filter models. However, there still is uncertainty as to how to design the multiple models used by a multiple model algorithm such as the IMM estimator.

In this paper, we investigate three maneuver modeling methods. These methods have been used by various authors for different applications [1] but no comparison of them has been reported, at least to the knowledge of the authors. As will be seen later in the paper, such comparison is valuable because it provides helpful information for those who have to decide which modeling method to use for the tracking problem at hands.

The first method, *variable process noise*, is the simplest, which has position and velocity as the target state and assumes two nearly constant velocity motion models. One constant velocity model has a small process noise (acceleration) for the quiescent mode without maneuver while the other constant velocity model with a large process noise is intended for the maneuvering mode.

The second method, *variable state dimension*, also has two models. One again is a nearly constant velocity model having position and velocity as the state with a small process noise for acceleration in the quiescent mode without maneuver. The maneuvering model now has acceleration as its state in addition to position and velocity.

The above methods belong to the design approach using two bandwidths. The quiescent filter has a small bandwidth to smooth out noise in non-maneuvering periods. The maneuvering filter has a large bandwidth to be responsive to maneuvers (and to noise in measurements as well). Strictly speaking, the more proper words to be used here should be "instantaneous bandwidth" or "processing gain" because of the time-varying nature of Kalman filter except in steady state.

The third method, *discrete acceleration input*, explicitly models maneuver dynamics wherein a set of models are used to cover different types of possible maneuvers and the uncertain intervals of maneuver parameters. This in fact falls into the design approach of matched filters. Many model set design methodologies are described in [9]. For simplicity, the particular maneuver considered in this paper is linear acceleration. The analysis can be readily extended to other types of maneuvers in higher dimensions.

Target maneuvers are relatively infrequent events of short durations. The multiple model algorithms use a transition probability matrix to characterize such maneuver events as switching between different target motion models or filters, each represented by a mode (model or filter) probability that the corresponding mode is the true one. When the same measurements that are used to update the target state are also used to determine the mode probabilities, the filters typically exhibit a

Report Documentation Page

1. REPORT DATE **JUL 2008**	2. REPORT TYPE	3. DATES COVERED **00-00-2008 to 00-00-2008**

4. TITLE AND SUBTITLE **Characteristic Errors of the IMM Algorithm under Three Maneuver Models for an Accelerating Target**	5a. CONTRACT NUMBER
	5b. GRANT NUMBER
	5c. PROGRAM ELEMENT NUMBER
6. AUTHOR(S)	5d. PROJECT NUMBER
	5e. TASK NUMBER
	5f. WORK UNIT NUMBER

7. PERFORMING ORGANIZATION NAME(S) AND ADDRESS(ES) **Air Force Research Lab, Wright Patterson AFB, OH, 45433**	8. PERFORMING ORGANIZATION REPORT NUMBER
9. SPONSORING/MONITORING AGENCY NAME(S) AND ADDRESS(ES)	10. SPONSOR/MONITOR'S ACRONYM(S)
	11. SPONSOR/MONITOR'S REPORT NUMBER(S)

12. DISTRIBUTION/AVAILABILITY STATEMENT
Approved for public release; distribution unlimited

13. SUPPLEMENTARY NOTES
11th International Conference on Information Fusion, June 30 ? July 3, 2008, Cologne, Germany.

14. ABSTRACT
see report

15. SUBJECT TERMS

16. SECURITY CLASSIFICATION OF:			17. LIMITATION OF ABSTRACT	18. NUMBER OF PAGES	19a. NAME OF RESPONSIBLE PERSON
a. REPORT **unclassified**	b. ABSTRACT **unclassified**	c. THIS PAGE **unclassified**	**Same as Report (SAR)**	**8**	

transient delay to react to errors developed in the predicted measurements and to distribute the errors to the states for correction (update). As part of the feedback mechanism, the transient errors are in fact a necessity. But the question is how much and for how long, which depends on the motion model(s) used by the filters and the filter design. Indeed, for the three models investigated in this paper, they exhibit characteristic errors throughout a maneuver, which are termed *n*-, *L*-, and *u*-shaped, respectively.

The total root mean squared (RMS) errors are typically used as a performance metric. For a maneuvering target, however, a time-equalized RMS (eRMS) may be more appropriate. The total and equalized RMS values are illustrated in this paper with computer simulations for the IMM under the three maneuver models for performance evaluation and filter tuning.

The paper is organized as follows. In Section 2, the three maneuver models for the IMM algorithm are formulated. In Section 3, the total RMS and equalized RMS are presented. Simulation scenarios and results are analyzed in Section 4 together with characteristic error shapes for the three models. In Section 5, filter tuning based on the total RMS vs. equalized RMS is described. Finally in Section 6 conclusions are offered together with future works.

2 Three Maneuver Models for IMM

After presenting the target truth model, this section describes the three maneuver models to be compared in this paper.

2.1 Target Truth Model

For simplicity and clarity, we will consider the one-dimensional (1D) case. Similar equations can be written for other dimensions of independent motions. The 1D target truth model is given by:

$$\begin{bmatrix} p_{t+1} \\ v_{t+1} \end{bmatrix} = \begin{bmatrix} 1 & T \\ 0 & 1 \end{bmatrix} \begin{bmatrix} p_t \\ v_t \end{bmatrix} + \begin{bmatrix} \frac{1}{2}T^2 \\ T \end{bmatrix} a_t \tag{1a}$$

$$z_t = \begin{bmatrix} 1 & 0 \end{bmatrix} \begin{bmatrix} p_t \\ v_t \end{bmatrix} + n_t \tag{1b}$$

The target state consists of position and velocity, i.e., $\mathbf{x}_t = [p_t, v_t]$', which are initialized at 0 m and 10 m/s, respectively. The sampling interval is $T = 1$ second. The simulation time is $t = 0$ to 120 seconds and an acceleration of $a_t = 5$ m/s^2 occurs during $t = 50$ to 70 seconds. The measurement noise standard deviation is $\sigma_n = 5$ m.

2.2 Variable Process Noise

In this method, the unknown acceleration with its change over time is dealt with by the following model:

$$\begin{bmatrix} x_{t+1} \\ v_{t+1} \end{bmatrix} = \begin{bmatrix} 1 & T \\ 0 & 1 \end{bmatrix} \begin{bmatrix} x_t \\ v_t \end{bmatrix} + \begin{bmatrix} \frac{1}{2}T^2 \\ T \end{bmatrix} w_t \tag{2}$$

where the process noise w_t is used to account for our knowledge (or lack of) about the maneuver acceleration. In the initial study, the measurement model is the same as the truth model (1b) with $\sigma_n = 5$ m.

Two motion models are used. The quiescent model has a small process noise $\sigma_w = 0.1$ m/s^2. This provides a nearly constant velocity model with which the filter will weight more on the historic data and motion model than the noisy measurements.

The maneuver model has a large process noise $\sigma_w = 5$ m/s^2, which has the effect of increasing the state estimation error covariance. It leads to a large Kalman filter gain that will weight more on latest measurements than historic data and the motion model. Instead of a Gaussian distribution with large variance in the maneuvering mode, the Levy distribution (a heavy tailed noise distribution) recently has been used in the IMM [14], which was shown to improve the IMM performance.

The two models are initialized with equal model probabilities and the Markov matrix of transition probabilities between the two models is given by:

$$\Pi = \begin{bmatrix} 0.9 & 0.1 \\ 0.1 & 0.9 \end{bmatrix} \tag{3}$$

The filter based on the nearly constant velocity model in (2) becomes the α-β filter in the steady state. For an α-β filter, the filter design as well as its performance is determined by the maneuver index defined as $T^2\sigma_w/\sigma_n$ [1, 6]. The filter gain is further related to the damping ratio (ζ) and natural frequency (ω_n), thus allowing the performance specification in terms of bandwidth and rising time [12].

What is implied in this method is that by opening up the bandwidth with a large gain, the filter will be able to correct predicted measurement errors and eventually catch up with the target after a maneuver. In other words, this method is based on the error-driven correction mechanism. A period of transient errors is evitable and in fact necessary for this method to work.

2.3 Variable State Dimension

In this method, two models are used. One is again the nearly constant velocity model with a small process noise $\sigma_w = 0.1$ m/s^2 as in (2). The other has an augmented state where the unknown acceleration is estimated explicitly. It is a nearly constant acceleration model:

$$\begin{bmatrix} p_{t+1} \\ v_{t+1} \\ a_{t+1} \end{bmatrix} = \begin{bmatrix} 1 & T & \frac{1}{2}T^2 \\ 0 & 1 & T \\ 0 & 0 & 1 \end{bmatrix} \begin{bmatrix} p_t \\ v_t \\ a_t \end{bmatrix} + \begin{bmatrix} \frac{1}{2}T^2 \\ T \\ 1 \end{bmatrix} w_t \tag{4}$$

where the process noise $\sigma_w = 5$ m/s^2 is set large. This process noise variance, added onto the estimation error covariance for this state component, determines the weighting factor, thus enabling fast estimation of a_t.

An alternative model for the acceleration in (4) is given below:

$$\begin{bmatrix} p_{t+1} \\ v_{t+1} \\ a_{t+1} \end{bmatrix} = \begin{bmatrix} 1 & T & \frac{1}{2}T^2 \\ 0 & 1 & T \\ 0 & 0 & \alpha \end{bmatrix} \begin{bmatrix} p_t \\ v_t \\ a_t \end{bmatrix} + \begin{bmatrix} 0 \\ 0 \\ \sqrt{1-\alpha^2} \end{bmatrix} w_t \tag{5}$$

where w_t is the noise for the acceleration state a_t with $\sigma_w = 5$ m/s^2.

The two models also have equal initial model probabilities and the Markov matrix of transition probabilities between the two models is the same as in (3).

This method estimates the underlying acceleration from the noisy data. When there is no maneuver, it tends to be influenced by measurement noise while trying to extract acceleration from it. When there is a maneuver, it takes time to obtain a correct estimate of (i.e., to converge to) the true value. This is also based on the error-driven correction mechanism and again it will have a period of transient errors.

2.4 Discrete Acceleration Input

The two methods described above are data-driven in the sense that it estimates the unknown acceleration from data. It does so by choosing different filter gains so as to weight either more on historic data (non maneuver) or latest measurements (maneuver). The third method studied here can be viewed as a *parallel search approach* (or a matched filter). It divides the uncertainty interval of acceleration into search points. Each search point is used as a discrete input. The model is written as:

$$\begin{bmatrix} p_{t+1} \\ v_{t+1} \end{bmatrix} = \begin{bmatrix} 1 & T \\ 0 & 1 \end{bmatrix}\begin{bmatrix} p_t \\ v_t \end{bmatrix} + \begin{bmatrix} \frac{1}{2}T^2 \\ T \end{bmatrix}(a_t + w_t) \tag{6}$$

where the process noise is used to account for modeling errors in maneuver acceleration with $\sigma_w = 0.1$ m/s^2.

For three discrete acceleration values (e.g., $a_t = 0, \pm a$), the three models also have equal initial model probabilities (1/3) and the Markov matrix of transition probabilities between the three models is given by:

$$\Pi = \begin{bmatrix} 0.9 & 0.05 & 0.05 \\ 0.05 & 0.9 & 0.05 \\ 0.05 & 0.05 & 0.9 \end{bmatrix} \tag{7}$$

When $a_t = 0$, (6) is exactly the same as the nearly constant velocity model in (2). When one of the discrete accelerations happens to match the true acceleration in (1a), (6) uses a small process noise in the maneuver mode as in the quiescent mode to obtain the best noise performance. However, when $a_t (\neq 0)$ is away from the true acceleration, a relatively large process noise can be used to account for the mismatch. Again, it is a tradeoff between noise performance and responsiveness.

This method can also be viewed as a *parametric approach* (it parameterizes the unknown acceleration) and the obvious question is how to divide the uncertainty interval of acceleration, that is, how many search points and their spacing and placement [9]. Over-parameterization (i.e., dense search points over an interval) is counter-productive, not only because it requires more computation but also closely-spaced models compete for limited data and make them "un-identifiable," thus biasing the average. In a sense, this violates the condition for the total probability theorem. A proper choice of model spacing needs to be commensurate with the underlying maneuver index [15].

3 Total vs. Equalized Root Mean Squared (RMS)

Performance metrics have been designed to evaluate estimation errors in position and velocity and to compare different tracking algorithms [3, 10]. However, different applications may have different requirements on different aspects of tracking performance. For example, track continuity with uniform tracking errors is important to surveillance. Targeting for weapon delivery requires better accuracy as the time-to-go becomes smaller. In a dense target environment, target maneuvers become important because it creates confusion and track swap for closely spaced targets.

Fig. 1 depicts a typical profile of estimation errors in terms of the RMS value as a function of time. For a maneuvering target, this RMS value may contain six segments as shown in Fig. 1:

   (1) Tracking errors due to initialization,

   (2) Tracking errors prior to maneuver,

   (3) Tracking errors after maneuver initiation,

   (4) Tracking errors during maneuver,

   (5) Tracking errors after maneuver termination, and

   (6) Tracking errors after maneuver.

The 2nd segment contains mostly the steady-state tracking errors and so does the 6th segment in the non-maneuver mode whereas the 4th segment contains the steady-state tracking errors in the maneuver mode. The 1st segment contains the initial transient errors; the 2nd segment contains the maneuver transient error, and the 5th segment contains the maneuver termination transient error. Since the steady-state and transient errors (prior to and after maneuvers) are quite different, the ratios of time intervals in these six segments are important factors affecting the total RMS valuation. This observation leads to the introduction of the time-equalized RMS value.
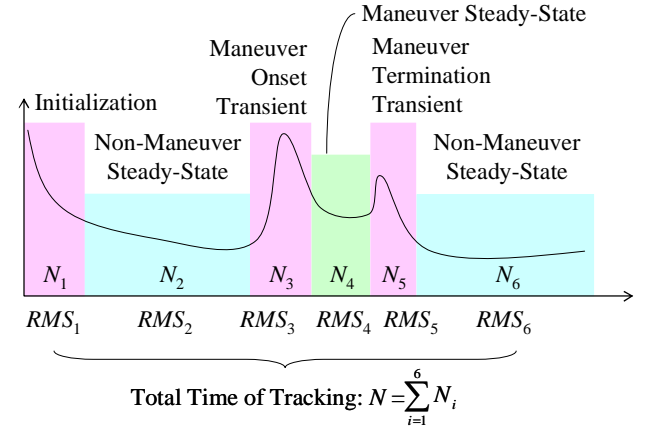
Fig. 1 Definition of Maneuver Events and Time-Weighted RMS Value

Since the maneuvers are relative infrequent events, the steady-state errors may become overwhelming, thus masking the transient errors in the total RMS (tRMS). The conventional total RMS can be written as:

$$RMS^2 = \frac{1}{N}\sum_{i=1}^{N}\varepsilon_i^2 = \sum_{j=1}^{6}\frac{N_j}{N}RMS_j^2 \tag{8}$$

where $\varepsilon_i = \hat{x}_i - x_i$ is the estimation error of the quantity x, N is the total number of RMS values, RMS_j is the total RMS value per segment, and N_j is the number of RMS values per segment.

Clearly the ratios N_j/N in (8) weight down those events of short durations. Yet, they are critical events which are important for tracking performance evaluation. A time-equalized RMS (eRMS) is defined as:

$$eRMS^2 = \frac{1}{6}\sum_{j=1}^{6}RMS_j^2 \tag{9}$$

where RMS_j is the total RMS value per segment.

To calculate the time-equalized RMS, one has to divide the target trajectory into maneuver events-related segments. This is rather simple in simulation where we know the truth about maneuvers. The concept of time-equalization can be applied to the normalized estimation error squared (NEES).

In (9), all the segments are given equal importance. However, if an application has different emphases on different segments, the above definitions can be adjusted accordingly. Metrics similar to the equalized RMS have been used in the past for performance

evaluation. Many authors have used tabulated RMS values, peak values, averages, peak to average ratios per segment for instance.

4 Three Maneuver Models in IMM

For the same simulation scenario, three IMM trackers using the three models described in Section 2 are applied. Although individual trackers are not optimized for the given scenario, their distinct behaviors are clear from the results, which are presented below with analysis.

Fig. 2 shows the position estimation error RMS for the three methods. Except for two small bumps after the start and end of the maneuver, the errors for Method 3 with discrete inputs (the green curve) remain flat with some small variations. The errors for Method 1 with variable process noise (the red curve) match those of Method 3 during the maneuver but smaller in other periods. In contrast, the errors for Method 2 with variable state dimension (the blue curve) are smallest (and smoothest) during the quiescent periods but largest right after the start of the maneuver. Both Methods 1 and 3 are slightly below this value whereas Method 2 is only below this level in quiescent periods.

The differences of these three methods can be seen more clearly in Fig. 3 for the velocity estimation error RMS. The errors for Method 3 with discrete inputs (the green curve) are smaller than other two methods during the maneuvering period. It is even smaller than quiescent periods. However, it still has two small bumps after the start and end of the maneuver. The errors for *Method 1* with variable process noise (the red curve) are smaller than those of Method 3 during quiescent periods but larger during the maneuver period. The errors for Method 2 with variable state dimension (the blue curve) are again smallest (and smoothest) during the quiescent periods but largest right after the start and end of the maneuver.

It is interesting to note that even though the three methods use the same quiescent model, their tracking performance in quiescent periods is quite different. This is because interacting of all models involved in the IMM. In the maneuver period, the errors of Method 1 with variable process noise (the red curve) are *n-shaped*, the errors of Method 2 with variable state dimension (the blue curve) are *L-shaped*, and the errors for Method 3 with discrete inputs (the green curve) are *u-shaped*.

The different behaviors are analyzed below in reference to a particular sample run as shown in Figs. 4 through 10. It is easy to understand why the errors of Method 1 with variable process noise are n-shaped, particularly for the velocity estimates. This is because the maneuver model of Method 1 does not include an acceleration state but is a constant velocity model with large process noise. It thus allows for larger and faster velocity updates than the quiescent counterpart.

This is shown in Fig. 4 for the innovations (i.e., the predicted measurement errors) for the quiescent model (the blue curve) and the maneuver model (the green curve). The two curves have about the same shapes during the quiescent periods but the green curve for the maneuver model is larger in size. The model probability for the quiescent model is therefore larger than the maneuver model as shown in Fig. 5. With the process noise $\sigma_w = 0.1$ vs. 5 m/s^2, the model probability is 0.6 vs. 0.4, not definitely in favor of the quiescent model, though.

In the maneuver period, the predicted measurement errors for the quiescent model are larger than those of the maneuver model, indicating large velocity estimates are used to catch up witch acceleration. This explains the presence of small bias in position estimate but large bias in velocity estimates. This is also reflected

in the model probabilities where the maneuver model is higher than the quiescent model over the maneuver period as shown in Fig. 5 (some pikes reach above 0.9 but there are lots of volatility).

The errors of *Method 2* with variable state dimension (the blue curve) are *L*-shaped as shown in Figs. 2 and 3 for the position and velocity estimates, respectively. The large errors, right after the maneuver, are due to the latency of the filter, which takes time (i.e., measurements) to estimate the underlying maneuver. Once this is done, the errors drop to the lowest level. Fig. 7 shows the model probability that rapidly rises to almost unity after the maneuver during which the position and velocity errors accumulate. The acceleration estimate is shown in Fig. 10.

Just like the fact that it takes time for the filter to estimate the acceleration, the filter also takes time to dump the acceleration estimate (discharge from an integrator) when the maneuver is terminated. That is the reason for the small rise in errors after maneuver termination. This is true for all higher-order models where integrators need to be charged and discharged. There are actually double actions going on. On the one hand, the maneuver model itself is estimating (or de-estimating) the acceleration which just vanishes. On the other hand, it transitions from the maneuver model to the quiescent model.

In the quiescent periods, the two models in Method 2 have 0.51 vs. 0.49 probabilities of being in favor as shown in Fig. 7. Their innovations are of about the same shape and size. This is different from Method 1 where the maneuver model has large errors. This is because in Method 2, the maneuver model attempts to estimate acceleration from noisy measurements. When there is no maneuver, its value is small as shown in Fig. 10 and it contributes little to prediction errors. In contrast, the maneuver model in Method 1 directly opens its processing gain and weights more on measurements, thus subject to noise.

The position errors for *Method 3* with discrete inputs (the green curve) are comparable to (slightly larger than) those of Method 1 with variable process noise (the red curve) as shown in Fig. 2. However, Method 3 has the lowest errors in velocity during maneuver except for the *u*-shaped spikes after the start and end of the maneuver. In a sense, the error spikes are necessary to flash out old estimates and to establish new estimates.

The innovations for the three models in Method 3 are shown in Fig. 8, which have about the same shape except they are shifted upwards and downwards by their discrete inputs. During quiescent periods, the measurement prediction errors stabilize around +20 and -20 m for the models with -5 and +5 m/s^2. Since these filters are mixed at each prediction and updating cycle, with the velocity error of 4 m/s, the equivalent time span is 2 to 3 updating intervals ($T = 1$ second) under 5 m/s^2 to develop such position errors.

The model probability for the quiescent model is close to 0.9 but with large spikes. The state mixed from the three models therefore produces the largest position and velocity errors among the three methods during the quiescent periods. However, during the maneuver period, the maneuver model with 5 m/s^2 prevails with the model probability close to unity as shown in Fig. 9. That is why the velocity errors are the smallest for Method 3.

Fig. 10 shows the acceleration estimates for Method 2 (blue) and Method 3 (green). Method 1 does not include an acceleration state so its curve (red) stays at zero. Method 3 produces the acceleration estimate rather close to the true value whereas Method 2 has delay and does not cover the entire duration. However, during the quiescent periods, the acceleration estimate of Method 3 remains volatile with large spikes corresponding to
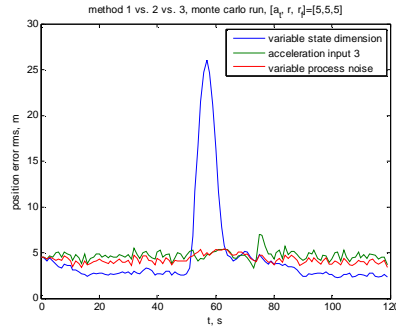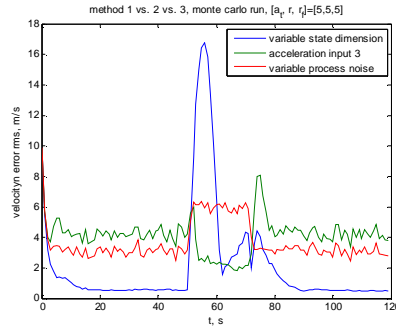
Fig. 2 Comparison of Position Errors
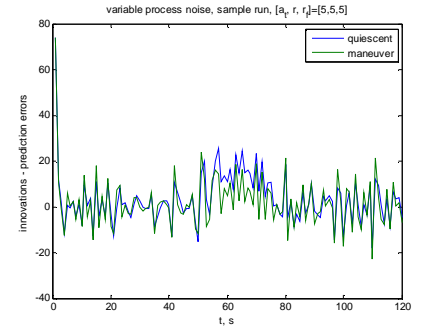

Fig. 3 Comparison of Velocity Errors

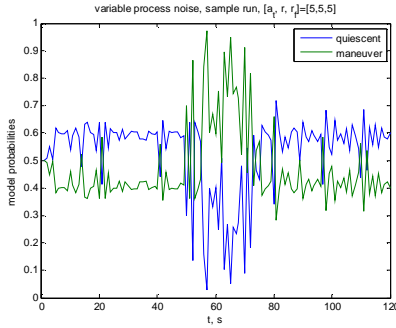Fig. 4 Innovations for Method 1
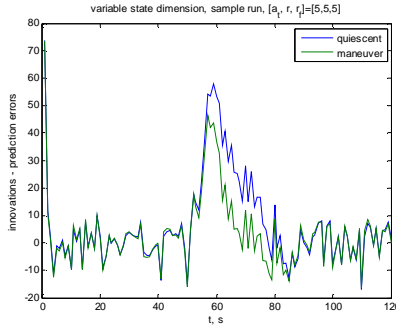

Fig. 5 Model Probabilities for Method 1
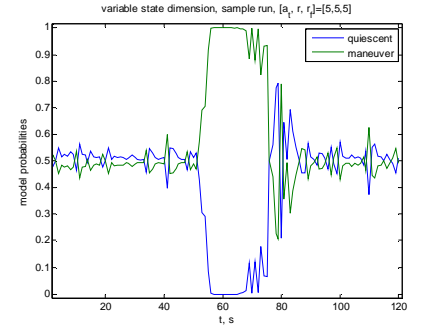

Fig. 6 Innovations for Method 2

Fig. 7 Model Probabilities for Method 2

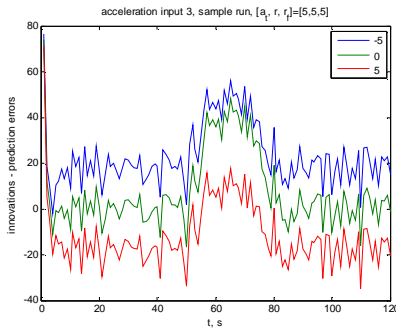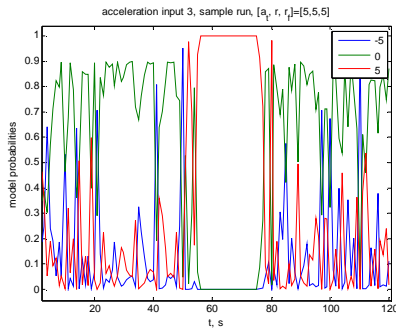Fig. 8 Innovations for Method 3
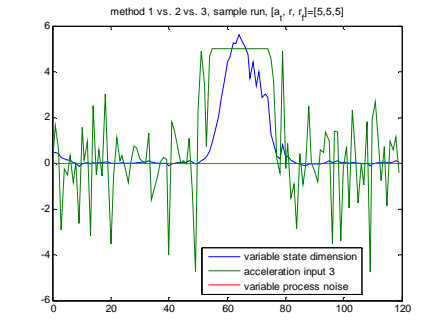

Fig. 9 Model Probabilities for Method 3

Fig. 10 Acceleration Estimates
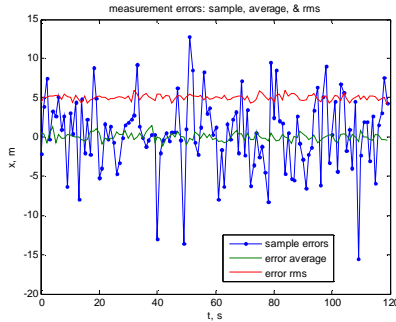

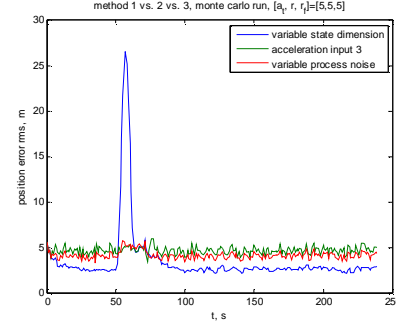Fig. 11 Measurement Errors (100 Runs)
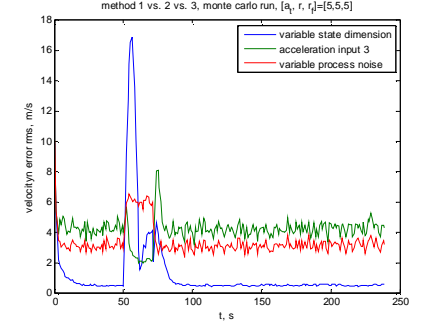

Fig. 12 Position Error RMS for Three Methods

Fig. 13 Velocity Error RMS for Three Methods

those in measurement noise. This makes it very responsive but also creates variations in model probabilities as well as in velocity and position estimates. In contrast, the acceleration estimate of Method 2 is close to zero and smoothing during quiescent periods. This makes its velocity and position estimates small but it is lack of responsiveness. These are examples showing tradeoffs between quiescent and maneuver periods.

Fig. 11 shows a sample measurement error, the mean value of measurement errors over the 100 Monte Carlo runs, and the RMS value of the measurement errors, which is close to the true value of $\sigma_n = 5$ m.

944

5 Evaluation and Tuning

By means of computer simulation, this section investigates the use of total RMS and equalized for performance evaluation and filter tuning.

5.1 Evaluation under Total & Equalized RMS

Consider the same simulation scenario presented in the previous section. Everything remains the same except for the simulation time, which is doubled now. That is, the relative maneuver period ratio is reduced from $20/120 = 16.7\%$ to $20/240 = 8.3\%$. For the simulation, the time interval is divided to two time zones: one is for the initial transition (from 1 to 8) and maneuver plus transition (from 50 to 78) and the other is for quiescent periods (from 9 to 49 and from 79 to 240).

Figs. 12 and 13 show the position and velocity error RMS values for the three methods, which are very similar to Figs. 2 and 3 over the initial half of simulation. The blue curve has large errors during maneuver periods but small errors otherwise. If the non-maneuver period is rather long, the maneuver errors in position and velocity are likely to be averaged out. This is indeed the case as shown in Table 1.

In Table 1, the first data column lists the total RMS for position estimates. Compared to Method 1 and Method 3, the value of Method 2 is slightly larger. It can be expected that if the simulation interval is increased a bit longer, this value will be smaller than the other two. However, in the third data column, the *time-equalized RMS* for position estimates of Method 2 is bigger than both Method 1 and Method 3 when the averaging effect is removed.

The averaging effect is more evident when we compare the velocity errors. The second data column shows that the total RMS of velocity estimates for Method 2 is smaller than Method 1 and Method 3. In contrast, the four data column shows that the time-equalized RMS of velocity estimates for Method 2 is bigger than Method 1 and Method 3.

Table 1 Total RMS and Time-Equalized RMS

	Total RMS		Time-Equalized RMS	
	Position	**Velocity**	**Position**	**Velocity**
Method 1	4.1218	3.5088	4.3540	4.3033
Method 2	4.9162	2.9171	7.8811	5.1741
Method 3	4.6369	4.2124	4.7219	4.2955

The use of time equalized RMS values eliminates the effect of time duration, which may otherwise mask infrequent events in calculating the total RMS. Furthermore, the equalized RMS is better suited to tune the IMM filter for maneuver scenarios as shown next. This is similar to sensitivity analysis of filter performance as a function of design parameters [5].

5.2 Tuning under Total and Equalized RMS

The parameters of individual filters using the three maneuvering models can be optimized in terms of the conventional total vs. time equalized RMS. For Method 1 with variable process noise, the key filter parameters are the process noise variances for the quiescent (q_0) and maneuvering (q_1) models. In the study, the true acceleration is $a_t = 5$ m/s^2. Both the true and model measurement variances are set to be the same as $\sigma = \sigma_t = 5$ m. The value for the quiescent process noise model is set to be $q_0 = 0.01$ m/s^2. The

value for the maneuver process noise model is tuned or varied as $q_1 = \kappa a_t$ for $\kappa = 0.1$ to 10.

Fig. 14 shows the two position error RMS values as a function of the tuning parameter κ. One is the conventional total RMS (blue) and the other is the equalized RMS (green). It is interesting to see that for the conventional total RMS, the minimum value is not at $\kappa = 1$ but some value smaller. In contrast, the minimum value for the equalized RMS is near $\kappa = 1$. Both total and equalized position error RMS values increase rapidly as κ becomes smaller because the maneuver model is less effective. It increases slowly as κ becomes bigger.

Fig. 15 shows the two velocity error RMS values as a function of the tuning parameter κ: the blue curve is the conventional total RMS (blue) and the green one is the equalized RMS. Similarly, the minimum value of the conventional total RMS is not at $\kappa = 1$ but somewhat smaller whereas the minimum value for the equalized RMS is near $\kappa = 1$. Both total and equalized position error RMS values increase rapidly as κ becomes smaller and it increases as κ becomes bigger.

In the second simulation, the true acceleration is again $a_t = 5$ m/s^2 and both the true and model measurement variances are set to be the same as $\sigma = \sigma_t = 5$ m. The value for the maneuver process noise model is set at $q_1 = 5$ m/s^2 while the value for the quiescent process noise model is tuned or varied as $q_0 = \kappa a_t$ for $\kappa = 0$ to 1.

Fig. 16 shows the two position error RMS values as a function of the tuning parameter κ for the conventional total RMS (blue) and the equalized RMS (green). Both the conventional total RMS and equalized RMS values decrease as κ becomes smaller. It flattens out after $\kappa < 0.05$ or $q_0 = 0.25$. The use of $q_0 = 0.01$ in the previous simulation seems reasonable.

Fig. 17 shows the two velocity error RMS values as a function of the tuning parameter κ. The same results hold. The equalized RMS (green) is larger than the conventional total RMS (blue) for both the position and velocity errors.

For Method 2 with variable state dimension, the key filter parameters are also the process noise variances for the two-state filter (q_0) and for the three-state filter (q_1). Again, the true acceleration is $a_t = 5$ m/s^2. The true and model measurement variances are set to be the same as $\sigma = \sigma_t = 5$ m. In the following simulation, the state process noise variance for one filter is fixed while for the other filter is tuned or varied as $q = \kappa a_t$ with κ.

In the first trial, the value for the two-state process noise model is set to be $q_0 = 0.01$ m/s^2. The value for the three-state process noise model is tuned or varied as $q_1 = \kappa a_t$ for $\kappa = 0$ to 10.

Fig. 18 shows the two position error RMS values as a function of the tuning parameter κ. One is the conventional total RMS (blue) and the other is the equalized RMS (green). For both the conventional total RMS and the equalized RMS, the minimum occurs around $\kappa = 0.2$ or $a = 1$ m/s^2. The position error RMS values increase rapidly as κ moves away from this minimum value of 0.2 and it starts to flatten out after $\kappa > 2$.

Fig. 19 shows the two velocity error RMS values as a function of the tuning parameter κ for the conventional total RMS (blue) and the equalized RMS (green). It exhibits the similar behavior as Fig. 18, that is, for both the conventional total RMS and the equalized RMS, the minimum occurs around $\kappa = 0.2$ or $a = 1$ m/s^2. The velocity error RMS values increase rapidly as κ moves away from this minimum value of 0.2 but it does not flatten out as quickly as the position error RMS values.
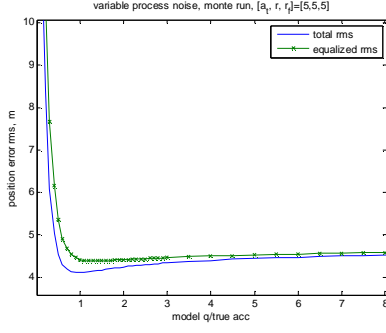
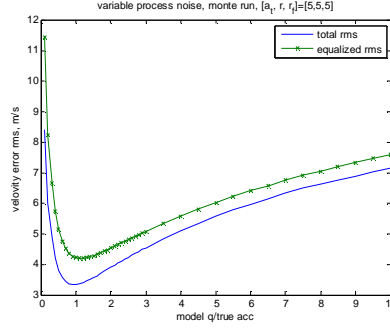Fig. 14 Position Errors over q_1 for $q_0 = 0.01$

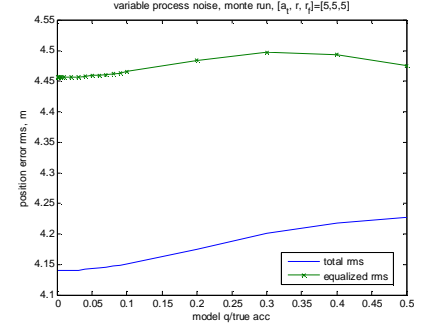Fig. 15 Velocity Errors over q_1 for $q_0 = 0.01$
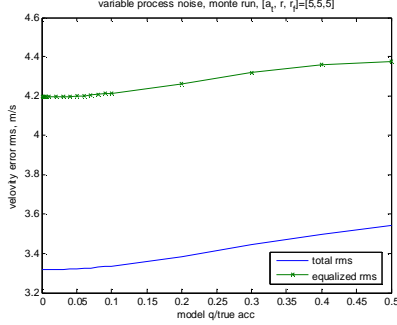

Fig. 16 Position Errors over q_0 for $q_1 = 5$

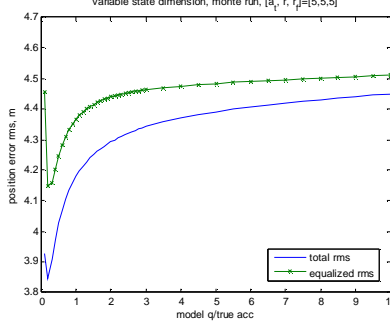Fig. 17 Velocity Errors over q_0 for $q_1 = 5$

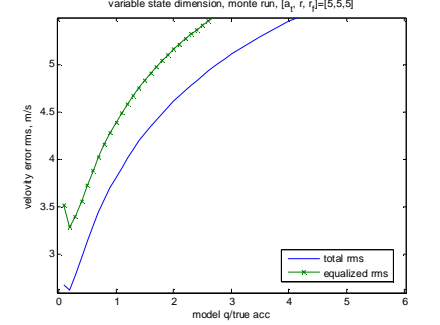Fig. 18 Position Errors over q_1 for $q_0 = 0.01$
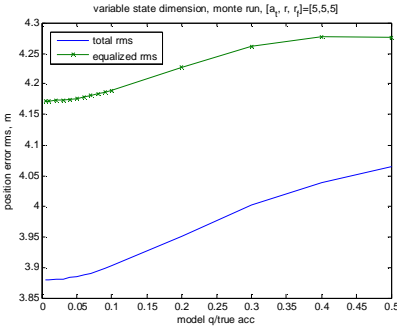

Fig. 19 Velocity Errors q_1 for $q_0 = 0.01$

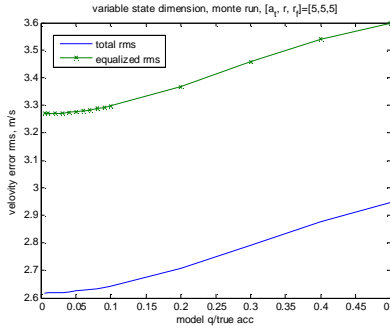Fig. 20 Position Errors over q_0 for $q_1 = 1$

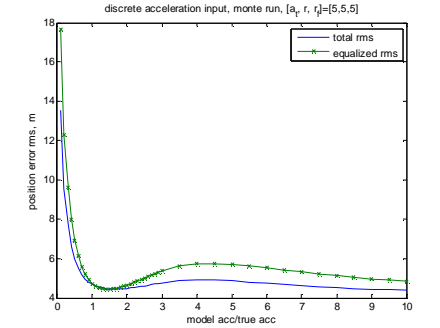Fig. 21 Velocity Errors over q_0 for $q_1 = 1$

Fig. 22 Position Errors over $\pm a$ for $q = 0.01$
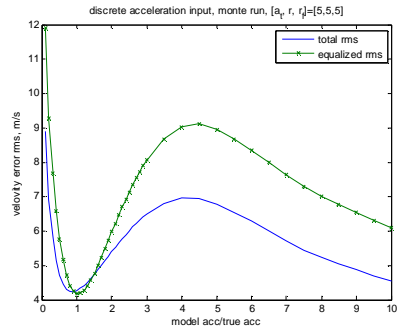

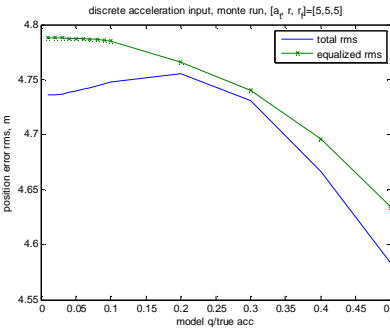Fig. 23 Velocity Errors over $\pm a$ for $q = 0.01$

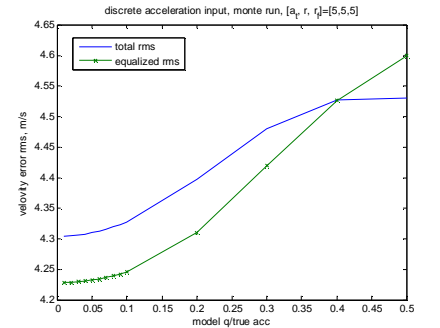Fig. 24 Position Errors over q for $a = \pm 5$

Fig. 25 Velocity Errors over q for $a = \pm 5$

In the second trial, the value for the three-state process noise model is set to be $q_1 = 1$ m/s^2. The value for the two-state process noise model is tuned or varied as $q_0 = \kappa a_t$ for $\kappa = 0$ to 0.5.

Figs. 20 and 21 show the position and velocity error RMS values as a function of the tuning parameter κ, respectively, where the conventional total RMS is blue-colored and the equalized RMS is green-colored. After $\kappa < 0.05$ or $a = 0.25$ m/s^2, the curves start to

flatten out. The use of $q_0 = 0.01$ m/s^2 seems to be a reasonable choice. The figures also show that the increase of RMS starts to reach a plateau (particularly for position) after $\kappa > 0.5$ or $a = 2.5$ m/s^2.

For Method 3 with discrete acceleration input, the key issue of filter design is determination of the number and selection of values for the discrete acceleration inputs. However, the process

noise variance is also important for the two-state filters with or without discrete acceleration input. The true acceleration is $a_t = 5$ m/s^2. The true and model measurement variances are set to be the same as $\sigma = \sigma_t = 5$ m.

In the first trial, the value for the two-state process noise model is set to be $q = 0.01$ m/s^2. Three acceleration input values are chosen for $a = 0$ (for quiescent without maneuver) and $\pm\kappa a_t$ with $\kappa = 0$ to 10 (for maneuver).

Fig. 22 shows the two position error RMS values as a function of the tuning parameter κ. One is the conventional total RMS (blue) and the other is the equalized RMS (green). For both the conventional total RMS and the equalized RMS, the minimum occurs around $\kappa = 1.5$ or $a = 7.5$ m/s^2 (the true value is $a_t = 5$ m/s^2). The position error RMS values increase rapidly as κ decreases but flatten out as κ increases.

Fig. 23 shows the two velocity error RMS values as a function of the tuning parameter κ for the conventional total RMS (blue) and the equalized RMS (green). It differs from Fig. 22 in two aspects. First, the conventional total RMS (blue) has its minimum at a κ value smaller than unity whereas the equalized RMS (green) has its minimum very near $\kappa = 1$. Second, both the RMS curves have a local maximum, which is around $\kappa = 4$ for the conventional total RMS (blue) and $\kappa = 4.5$ for the equalized RMS (green).

As κ goes smaller, the discrete acceleration input to the maneuver models becomes smaller. The maneuver models degenerate into non-maneuver filters. This explains why the RMS value increases rapidly as κ decreases. On the other hand, when κ becomes bigger, the true maneuver may become closer to the no-maneuver model than the maneuver models with very large acceleration input. As a result, the large acceleration models are excluded from the combined filter output where the non-maneuver model is dominant.

In the second trial, the discrete acceleration input is set to be $a = \pm 5$ m/s^2. The value for the process noise variance (equal for both maneuver and non-maneuver models) is tuned or varied as $q = \kappa\, a_t$ for $\kappa = 0$ to 0.5.

Figs. 24 and 25 show the position and velocity error RMS values as a function of the tuning parameter κ, respectively, where the conventional total RMS is blue and the equalized RMS is green. In general, the position error RMS values decrease with increased κ whereas the velocity error RMS values increase with increased κ. The increase of position error RMS and the decrease of velocity error RMS flatten out for small κ. It is reasonable to choose $q = 0.01$ as the process noise variance.

Additional results for filter behaviors under model mismatches can be found in [18].

6 Conclusions

In this paper, we investigated the use of three maneuver models in the IMM algorithm for maneuvering target tracking and showed their characteristic errors. More specifically, right after the start and ending of a maneuver, the errors of the model with variable process noise are n-shaped, the errors of the model with variable state dimension are L-shaped, and the errors for the model with discrete inputs are u-shaped. The performance and tuning of these models were compared under the total vs. equalized RMS errors.

It is readily to extend the observations made on the 1D case in this paper to the 2D and 3D cases and from linear accelerations to turning and other more complicated maneuvers. For example, the unknown turn rate in the coordinated turn maneuver can be treated in much the same way as the unknown linear acceleration studied in this paper. In addition, it is interesting to apply the three maneuver models to other multiple model estimation algorithms. Because of their distinct behaviors during quiescent and maneuvering periods, it might be valuable to combine the multiple model estimation algorithms with different models, resulting in "methodology fusion." To reduce transient errors, the fusion with other sources of information such as the target maneuver indicator derived from the target's range-Doppler images [16, 17] is under investigation [18].

References

[1] Y. Bar-Shalom and X.R. Li, *Multitarget-Multisensor Tracking: Principles and Techniques*, YBS Publishing, Storrs, CT, 1995.

[2] Y. Bar-Shalom, Subhash Challa, and H.A.P. Blom, "IMM Estimator versus Optimal Estimator for Nybrid Systems," *IEEE Trans. Aerospace and Electronic Systems*, 41(3), July 2005.

[3] E.P. Blasch, A. Rice, and C. Yang, "Relative Track Metrics to Determine Model Mismatch," *Proc. of the SPIE: Signal and Data Processing of Small Targets*, O.E. Drummond (Ed.), Vol. 6236, June 2006.

[4] H. Blom and Y. Bar-Shalom, "The Interacting Multiple Model Algorithm for Systems with Markovian Switching Coefficients," *IEEE Trans. on Automatic Control*, 33(8), 1988.

[5] A. Gelb (Ed.), *Applied Optimal Estimation*, The MIT Press, Cambridge, MA, 1974.

[6] P.R. Kalata, "The Tracking Index: A Generalized Parameter for α–β and α–β–ρ Target Trackers," *IEEE Trans. Aerospace and Electronic Systems*, 20(2), March 1984.

[7] T. Kirubarajan and Y. Bar-Shalom, "Kalman Filter versus IMM Estimator: When Do We Need the Latter?" *IEEE Trans. Aerospace and Electronic Systems*, 39(4), October 2003.

[8] X. R. Li and V. P. Jilkov, "A Survey of Maneuvering Target Tracking—Part V: Multiple-Model Methods," *IEEE Trans. Aerospace and Electronic Systems*, 41(2), 2005.

[9] X. R. Li, "Engineer's Guide to Variable-Structure Multiple-Model Estimation for Tracking," Y. Bar-Shalom and W. D. Blair, eds., Multitarget-Multisensor Tracking: Applications and Advances, Vol. 3, Chapter 10, Artech House, Boston, 2000, pp. 499-567.

[10] X.R. Li and Z.L. Zhao, "Evaluation of Estimation Algorithms. Part I: Local Performance Measures," *IEEE Trans. Aerospace and Electronic Systems*, November 2004.

[11] P. Mayabeck, *Stochastic Models, Estimation, and Control*, Volume 1, Academic Press, Inc, 1979.

[12] J.H. Painter, D. Kerstetter, and S. Jowers, "Reconciling Steady-State Kalman and Alpha-Beta Filter Design," *IEEE Trans. Aerospace and Electronic Systems*, 26(6), November 1990.

[13] R. R. Pitre, V. P. Jilkov, and X. R. Li, "A Comparative Study of Multiple-Model Algorithms for Maneuvering Ttarget Tracking," *Proc. 2005 SPIE Conf. Signal Processing, Sensor Fusion, and Target Recognition XIV*, Orlando, FL, March 2005

[14] A. Sinha, T. Kirubarajan, and Bar-Shalom, "Application of the Kalman-Levy Filter for Tracking Maneuver Targets," *IEEE Trans. Aerospace and Electronic Systems*, 43(3), July 2007.

[15] C. Yang and E. Blasch, "Analytic Tools to Improve Maneuvering Target Tracking," *Proc. of National Symp. on Sensor Data Fusion*, McLean, VA, May 2006.

[16] C. Yang and E. Blasch, "Estimating Target Range-Doppler Image Slope for Maneuver Indication," Proc. of SPIE Defense and Security 2008: Signal Processing, Sensor Fusion, and Target Recognition XVII, March 2008, Orlando, FL.

[17] C. Yang, W. Garber, R. Mitchell, and E. Blasch, "A Simple Maneuver Indicator from Target's Range-Doppler Image," *Fusion'2007*, Quebec, Canada, July, 2007.

[18] C. Yang, *Hybrid Kalman Particle Filter for Ground Target Tracking*, Technical Reports to AFRL/RYAA, 2008.